Anionic phospholipids stimulate the proton pumping activity of the plant plasma membrane P-type H^+-ATPase

Laura C. Paweletz[1], Simon L. Holtbrügge[2], Malina Löb[1], Dario De Vecchis[2], Lars V. Schäfer[2,*], Thomas Günther Pomorski [1,3,*], Bo Højen Justesen [1,*]

[1] Department of Molecular Biochemistry, Faculty of Chemistry and Biochemistry, Ruhr University Bochum, 44780 Bochum, Germany

[2] Center for Theoretical Chemistry, Faculty of Chemistry and Biochemistry, Ruhr University Bochum, 44780 Bochum, Germany

[3] Department of Plant and Environmental Sciences, University of Copenhagen, 1871 Frederiksberg C, Denmark

*Authors for correspondence

Bo Højen Justesen, Email address: Bo.Justesen@ruhr-uni-bochum.de; Thomas Günther Pomorski, Email address: Thomas.Guenther-Pomorski@ruhr-uni-bochum.de; Lars V. Schäfer, Email address: Lars.Schaefer@ruhr-uni-bochum.de

Running title: Lipid effect on the plant H^+-ATPase activity

Keywords: liposome, H^+-ATPase, lipid-protein interaction, molecular modeling, proton pump

Abstract:

The activity of membrane proteins depends strongly on the surrounding lipid environment. Here, we characterize the lipid stimulation of the plant plasma membrane H^+-ATPase AHA2 upon purification and reconstitution into liposomes of defined lipid compositions. We show that the proton pumping activity of AHA2 is stimulated by anionic phospholipids, especially by phosphatidylserine. Molecular dynamics simulations revealed several preferential contact sites for anionic phospholipids in the transmembrane domain of AHA2. These contact sites are partly conserved across functionally different P-type ATPases from several organisms, suggesting a general regulation mechanism by the membrane lipid environment. Our findings highlight the fact that anionic lipids play an important role in the control of H^+-ATPase activity.

Introduction

Membrane proteins of the P-type ATPase family are key players in the formation and maintenance of electrochemical gradients across cellular membranes through primary, active transport of ions. Consequently, they are involved in numerous vital biological processes including signal transduction, nutrient transport, and cell–cell communication (1–3). Based on sequence similarity and substrate specificity, the P-type ATPase family is divided into five distinct subfamilies (P1–P5, for reviews see 4, 5). Prominent examples are the Na^+/K^+-ATPase (P2), which generates the electrochemical gradients for sodium and potassium, and the sarcoplasmic reticulum Ca^{2+}-ATPase (P2), which pumps calcium from the cytosol into the lumen of the sarcoplasmic reticulum of skeletal muscle cells. Plasma membrane H^+-ATPases belong to the P3 subfamily, and are only found in plant, fungi and protozoa (reviewed in 6, 7). They transport H^+ ions out of the cell to generate and maintain an electrochemical H^+ gradient across the plasma membrane, which drives nutrient uptake and is involved in intracellular pH regulation, stomatal opening, and cell growth (8).

In accordance with their vital cellular functions, P-type ATPases are commonly subject to tight regulation, which for members of the P3 subfamily is mediated through autoinhibitory regulatory domains (R-domains) located at the N- and C-termini (9, 10). The impact of these domains on pumping activity is controlled by both post-translational modifications and accessory proteins. Of the eleven H^+-ATPases found in the model plant *A. thaliana*, the isoform 2 (*Arabidopsis thaliana* H^+-ATPase isoform 2; AHA2) is the most extensively studied. Phosphorylation of residues in the R-domain of AHA2 induces binding of regulatory proteins that are believed to displace the autoinhibitory R-domains from the catalytic domain, resulting in activation of the pump (9, 10). In addition, lysophospholipids have been shown to activate the plant H^+-ATPase by a mechanism involving both cytoplasmic terminal domains of the transporter (11, 12). Further evidence for a role of phospholipids in the regulation of H^+-ATPases comes from studies at the level of purified proteins either in detergent micelles or proteoliposomes. In these studies, the presence of anionic lipids stimulated the activity of several plant and fungal plasma membrane H^+-ATPases, but it remains unclear whether this mode of regulation involves the C-terminal regulatory domain (13–16).

In this study, we used a C-terminal truncated version of AHA2 lacking the regulatory R-domain (9, 10). Removal of the R-domain renders the enzyme to be in a constitutively active state (17), enabling us to study the impact of the lipid environment on the activity of AHA2 through reconstitution of the purified protein into liposomes of defined phospholipid composition. Measuring the H^+-transport activity of the reconstituted AHA2 showed that it was sensitive to the lipid environment and specifically stimulated by phosphatidylserine (PS), and to a minor degree by two other anionic phospholipids, phosphatidylglycerol (PG) and phosphatidic acid (PA). In concert with these observations, molecular dynamics (MD) simulations identified specific lipid interaction sites, which involve protein residues that are conserved across a broad range of P-type ATPases.

Results

***AHA2 activity is stimulated by anionic phospholipids*.** To investigate the role of the lipid environment on AHA2 activity, the protein was purified and reconstituted into preformed liposomes composed of different binary lipid compositions (Fig. 1B). Thin layer chromatography and SDS-PAGE analysis confirmed efficient removal of detergent as well as the lipid composition and protein content of each preparation (Suppl. Fig. S1). Estimation of membrane orientations of AHA2 in the different lipid compositions did not show any significant differences: about 80% of the proteins had the cytoplasmic portion orientated to the outside (Suppl. Fig. S2).

The resulting proteoliposomes were tested for proton pumping activity using 9-amino-6-chloro-2-methoxyacridine (ACMA) as a fluorescent ΔpH probe (Fig. 1A). For all proteoliposome preparations, immediate fluorescence quenching was observed after incubation with Mg^{2+}-ATP, which was promptly recovered after the subsequent addition of the protonophore m-chlorophenylhydrazon (CCCP), demonstrating that the reconstituted AHA2 was functional and able to generate a pH gradient (exemplary trace shown in Fig. 1C). The initial slope is used as estimate for the proton pumping rate, as no significant transmembrane proton leakage is yet assumed due to buildup of the gradient over time. Analysis of the initial rates of proton pumping, revealed pronounced differences in AHA2 activity between the different lipid compositions (Fig. 1D). Whereas the addition of 30 mol% of the non-bilayer lipid phosphatidylethanolamine (PE) to phosphatidylcholine (PC) did not affect AHA2 activity relative to pure PC, a significant and specific high proton pumping rate was observed for AHA2 in the presence of anionic species at the same concentration (Fig. 1D). Noticeably, an almost two times higher proton pumping rate was recorded for PS containing proteoliposomes compared to PG and PA (5.4-fold versus 2.2 to 2.4-fold compared to PC only). Similarly, AHA2 reconstituted in the ternary lipid mixture PC:PE:PS (45:45:10), displayed a 3.2-fold increase in the proton pumping rate (Suppl. Tab. S1).

To further characterize the effect of anionic lipids on AHA2 activity, proteoliposomes with intermediate lipid compositions were prepared and tested for proton pumping activity using ACMA. As shown in Figure 2, an increasing amount of PA and PG in the proteoliposomes resulted in an increased AHA2 proton pumping activity relative to pure PC of 3.3 and 2.6-fold at 20 mol%, respectively. A further increase in the amount of PA and PG resulted in a slight decrease of AHA2 activity (albeit not statistically significant). In contrast, with increasing amounts of PS, the proton pumping rate of AHA2 increased 4.6-fold over PC alone, reaching maximal activity at ~30 mol% PS in the range tested. These results indicate a specific stimulation of AHA2 proton pumping activity by phosphatidylserine (Suppl. Tab. S1 - 4).

Anionic phospholipids interact favourably at distinct AHA2 sites

To investigate the molecular underpinnings of the observed stimulation of the H^+ pumping activity by PS, multi-microsecond molecular dynamics (MD) simulations were carried out using the coarse-grained MARTINI model. AHA2 was simulated in two different lipid bilayers composed of PS:PC (10:90 molar ratio) and PS:PC:PE (10:45:45 molar ratio), respectively. The two-dimensional lipid densities around AHA2 (Fig. 3A) revealed that, compared to the neutral lipids, anionic PS strongly accumulates in the annulus around the transmembrane domain of AHA2. The PS lipids preferentially accumulate at distinct sites (Fig. 3A, sites A-E).

The majority of the identified sites are located on the cytosolic side of the membrane (Fig. 3A, sites A, B, D and E).

Next, to more closely investigate the identified sites, the contacts between individual AHA2 residues and the phospholipid head groups were analyzed (Fig. 3B, Tab. S5). All the lipid enrichment sites A-E were found in the contact analysis. Most of the identified PS-contacting residues are positively charged Lysine or Arginine residues. To provide even deeper insights into the lipid-protein interactions at the structural level, three-dimensional lipid densities were computed from the MD simulation trajectories (Fig. 3C). In congruence with the above results, well-defined density maxima of anionic PS lipids were consistently found at the distinct positions, with the most pronounced density at site A_1. Notably, the 3D density analysis not only shows sharp density peaks for the PS head groups but also partly for the associated lipid tails, which tend to become more disordered towards the membrane midplane. In the following, the 2D and 3D lipid densities are further analyzed and discussed in conjunction with the protein-lipid contacts to elaborate the positioning and importance of individual protein-lipid interaction sites in more detail.

The identified interaction site A_1 is located close to the cytoplasmic end of transmembrane helix M10, just next to the (missing) R-domain, and site A_2 is adjacent to it, located at the cytoplasmic end of M3 and M7. The two sites share the contact residues ^{M7}K705, ^{M7}L706, and ^{M7}K707, whereas residues ^{M10}R842 and ^{M3}K238 are assigned to the individual sites A_1 and A_2, respectively. Site B is located at the unstructured loop connecting M1 and the actuator (A) domain, in proximity to a proposed solvent tunnel and the cytoplasmic proton entry site leading to the proton acceptor pair D684 and N106 (18–21). The lipid contact analysis revealed ^{M1}K57 and ^{M1}K60 as contact residues for site B. Interestingly, both residues have previously been suggested as possible lipid interaction sites on the basis of MD simulations (18). The identified exoplasmic interaction site C is close to the M3-M4 loop and encompasses lipid-contact residues ^{M3}Q266, ^{M3}R267, ^{M3}R268, ^{M4}Y270 and ^{M4}R271. The nearby and conserved ^{M1}D92/^{M1}D95 were speculated by Pedersen et al., 2007 to be involved in proton release (19). Since site C is in the exoplasmic leaflet, its relevance for AHA2 activation in asymmetric biological membranes is presumably low. Site D returned the single contact residue ^{M6}K692. It is located near the cytoplasmic end of M6 and does not significantly favor PS over neutral lipids (Tab. S5). Thus, protein-lipid interactions at site D are unlikely to be directly linked to stimulation of AHA2 by anionic lipids, but they might be of structural importance. Finally, interaction site E is located next to site D at the end of M6, with contact residue ^{M6}R694. The positively charged arginine is surrounded by other charged residues (K692, D693, K696) and is located next to a water cavity proposed to be involved in cytoplasmic proton entry to the proton binding site (D684) (18–21). The MD simulations yield similar results for interaction sites A_1, A_2, and E in both lipid mixtures studied (PS:PC and PS:PE:PC). For sites B, C, and D, the lipid densities and contact probabilities are lower in the ternary mixture. The most pronounced preferential lipid interactions are consistently found at site A_1.

Binding sites for anionic lipids are partially conserved among plant and fungal H^+-ATPases

To investigate whether the putative anionic lipid-protein contact sites A, B, C, D and E are conserved, protein sequences from a range of P-type ATPases were aligned (see Methods). For this analysis, sequences from two isoforms of *A. thaliana* proton pumps (AHA1-2), plant

proton pumps from tobacco (*Nicotiana plumbaginifolia*) and rice (*Oryza sativa subsp. Japonica*), yeast proton pumps from Baker's yeast (*Saccharomyces cerevisiae*) and *Neurospora crassa*, and rabbit Ca^{2+}-ATPase (SERCA) and shark Na^{+}/K^{+}-ATPase (Na,K) were selected for sequence alignment.

In general, P-type ATPases overall show very low sequence similarity between structures (Fig. 4B, and Fig. S3). (4, 22). From sequence alignment of the regions covering the lipid contact sites, the only interaction site fully conserved among all the analyzed structures is the ^{M10}R842 in A_1. Curiously the site A_1 has previously been proposed as a lipid interaction site in SERCA (R989) with a bound lipid (PE) identified in the crystal structure of 4UU1, 2AGV, 3AR3-7 and 3W5C (23–26). Additionally the R1003/R1011 in the pig/shark Na,K-ATPase (3WGV), located only 5 amino acids downstream from the fully conserved ^{M10}R842 in AHA2, has also been identified as a sub site of a lipid binding site at M8-10 (27, 28). Both the individual interaction sites as well as several flanking residues were found to be well conserved among the sequences for the analyzed plant proton pumps; of the individual lipid interaction sites only the ^{M3}K238 (A_2) and the ^{M7}K707 (A_1/A_2) were found to be different, with a threonine in rice PMA (A_2) and an Ala in tobacco PMA (A_1/A_2). Still, a pair of lysines is located in M8/M9 that is supposed to be an lipid interaction site based on the crystal structure and native MS (29). For the two yeast proton pumps, only the ^{M1}K60 in site B was fully conserved, with several flanking residues found to be conserved in sites A_1/A_2, A_2, B, and D/E. As expected, the number of conserved residues found in both the lipid-protein interaction sites, as well as adjacent residues, were considerably lower in the SERCA and Na,K pumps than among the analyzed proton pumps. For both pumps, the only fully conserved interaction site is ^{M10}R842 at site A_1, while site D/E is partially conserved at ^{M6}R694.

Discussion

As integral membrane proteins, P-type ATPase interact intimately with membrane lipids, and several specific lipid interactions have been reported. For P-type ATPase cation transporters, one example of lipid interaction is the association of the *S. cerevisiae* Pma1 with lipid raft domains and its interaction with sphingolipids, required for delivery to the plasma membrane (for review see 30). Particularly anionic phospholipids have been shown to affect the activity of several P-type ATPases, including the activity of Ca^{2+} and Na^+/K^+ transporting P2 ATPases as well as several H^+ pumping P3 ATPases (14, 31–33). The findings presented in this work further emphasize the role of anionic phospholipids on the proton pumping activity of the plant H^+-ATPase AHA2. Reconstitution of purified AHA2 into liposomes with defined lipid composition enabled the specific characterization of the potential role of lipids on the transporter outside the complexity of the native environment. The proton pumping activity of the resulting AHA2-containing proteoliposomes was shown to vary depending on the presence of anionic lipids, with the strongest stimulation by PS. These results are in line with previous reports on plant H^+-ATPases, where anionic lipids have been found to stimulate ATPase and/or proton pumping activity of detergent extracted membranes containing H^+-ATPases from maize, *Zea mays*, rice, *Oryza sativa*, and mung bean, *Vigna radiata* (13, 16, 34). Depending on the origin of the pump and the varying extraction protocols, the order of stimulation varied. For example, *Z. mays* PMA was stimulated to the highest degree by PA (2-fold compared to PC or PE) , followed by PG and PS on the same level as the complex lipid extract lecithin (1.6 – 1.7 -fold) (13), while *O. sativa* PMA was stimulated the strongest by lecithin (2-fold) and PS (1.5-fold), while PG and PA showed no increased activity over PC (34). Furthermore, no stimulation by PA or PE was found for *V. radiata* PMA, but an increase in activity was observed in the presence of PS and PG which was in the same order of magnitude as PC (3 to 1.5-fold over no lipids added) (16, 35). A recent study also found PS stimulation of the proton pumping activity for H^+-ATPases in plasma membrane vesicles from *A. thaliana* (15). To our knowledge, the herein shown results constitute the first example of proton pumping stimulation by anionic lipids of a purified and reconstituted plant plasma membrane H^+-ATPase.

Of the tested anionic lipids, PS showed the strongest stimulation of H^+ pumping as compared to PA and PG, implying a specific lipid-protein interaction. Consequently, several regions with an increased anionic lipid density were identified using coarse-grain molecular dynamics simulations of AHA2 embedded in different membrane compositions, each containing 10% of the anionic phospholipid phosphatidylserine in a background of neutral lipids. The identified sites were all located at the lipid-protein interface, and potential residues for anionic lipid-protein interaction sites were subsequently found by contact analysis. Of the five sites located at the cytoplasmic side, site B with ^{M1}K57 and ^{M1}K60 has previously been identified as possibly involved in the function and regulation of P-type ATPases (18). A segment covering both residues is almost entirely conserved in the plant proton pumps as shown in the multiple sequence alignment (Fig. Suppl S3), with ^{M1}K60 also being conserved in the two yeast proton pumps *S. cerevisiae* Pma1 and *N. crassa* Pma1. The two residues have previously been identified in the report on the refined crystal structure of AHA2 by Focht et al. (2017) as possible interaction sites for anionic phospholipids. Furthermore, MD simulations showed this region to partition into the membrane interface, inducing a local depression speculated to facilitate solvent access to the H^+ binding site (D684-N106 pair) (18). Similar observations have recently been made for the structures of *S. cerevisiae* Pma1 (36) and *N. crassa* Pma1, solved in the auto-inhibited E1 conformation (37). In *N. crassa* Pma1, M1 is buried deeply within the membrane facilitating cytosolic access towards the H^+ binding site, with K115, corresponding

to ^{M1}K60 in AHA2, oriented to the lipid headgroup-aqueous interface as a so-called snorkeling residue (37). A similar proton access pathway is found in the structure of *S. cerevisiae* Pma1, where additionally the proton pumping cycle is found to involve movement of M1 towards the cytosolic leaflet of the bilayer in the E2P state (36). Such re-arrangement of M1 is also supported by a proposed mechanism of proton transport in *N. crassa* Pma1 based on a SERCA homology model (37). In this context, a possible role of the anionic lipid binding site B could be to aid in the movement of M1 towards the cytosolic leaflet, accelerating the conformational changes required for occlusion of the proton binding site followed by exposure to the exoplasmic site and thereby increasing the proton pumping rate.

In addition to the structural data detailed above, mutational studies on residues located in the region of site B has also been reported. An E167K mutation in the related *A. thaliana* Ca^{2+}-ATPase ACA2, corresponding to ^{M1}K60 in AHA2, resulted in a deregulated pump with activity similar to the activated state (38). A similar result was observed for a P72A mutation in *N. plumbaginifolia* Pma2, corresponding to ^{M1}P68 in AHA2, which is conserved in P3 ATPases and is responsible for the 90° kink in the M1 speculated to facilitate solvent access to the H^+-binding site (39, 40). This mutation also removes the sensitivity and stimulation by LysoPC. Both residues have been proposed to be interacting with the autoinhibitory C-terminal regulatory domain, although while a similar P68S mutation in AHA1 resulted in increased proton pumping activity, it did not seem to inhibit interaction of the R-domain with the cytosolic domains (41, 42). Considering the molecular dynamics simulations shown in this work, an alternative explanation for the observed activation could be an altered lipid interaction site in this region. This would also be in line with our observation of a lipid induced proton pumping stimulation of AHA2 devoid of the R-domain. Further mutational studies are required to investigate such an effect.

Along with the above-mentioned residues at site B, mutations of the ^{M4}D272A and ^{M4}D275A located adjacent to the lipid-protein contact residues at site C seems to be the only examples of mutagenesis studies of the putative anionic interaction sites identified in this work (43). However, the two mutations did not show any effect on the ability of AHA2 to complement the native yeast proton pump. Site C is the sole identified anionic lipid enrichment site in the exoplasmic leaflet and is located in close proximity to the proposed proton exit pathway with ^{M4}D272 and ^{M4}D275 at the periphery of the contact site buried deeper into the membrane near a putative cation binding site identified by (18, 19, 43). Given the proximity of interaction site C to the putative proton exit pathway, one possible function of anionic lipids in this region could be to facilitate the attraction of protons during the exposure of the H^+-binding site to the exoplasmic space. A similar role for the attraction of protons in the E1 conformation to the H^+-binding site, could also be envisioned for sites A_2 and B.

The recently reported structures of the yeast proton pumps *S. cerevisiae* Pma1 and *N. crassa* Pma1 revealed a hexamer arrangement, confirming previous reports on the oligomerization of P3 type ATPases (36, 37, 44, 45). Similarly, several studies have also reported on the oligomerization of plant proton pumps (42, 46). Even though the exact role of oligomerization remains unknown, there are indications that for plant proton pumps, activation by 14-3-3 proteins involve the formation of hexamer complexes (42), while for the yeast proton pump *N. crassa* Pma1 autoinhibition is enhanced or possibly even dependent on the hexamer arrangement (37). Based on the yeast proton pump structures, interaction sites A_1, A_2 and C could potentially be involved in mediating the formation of hexamers. In the structure of the *S. cerevisiae* Pma1, lipids in the exoplasmic leaflet were found to bind to M3/M7, at the interface between two monomer units, near the location of site C. Unfortunately, the lipid head groups

were not resolved, and therefore their exact composition remains unknown. MD simulations (37) on the *N. crassa* Pma1 identified two putative lipid binding sites near our site A_1 (Site I) and site C (Site II) also located at the interface of two monomers. Whereas site I showed an accumulation of anionic PS, in accordance with the observations from the MD simulations on AHA2, site II showed preferred binding of PC. The identification of a putative PS binding site for *N. crassa* Pma1 fits well with reports showing the activity of the yeast proton pump to depend on the presence of anionic lipids (32) and the PS enrichment in *N. crassa* Pma1 containing polymer nanodiscs (47). The effects of anionic lipids on the function and regulation of P3 ATPases could very well entail several of the above proposed interactions, and might furthermore differ between yeast and plant proton pumps despite the similarities found in the putative anionic lipid binding sites. Based on the putative lipid binding sites identified in this work, future mutagenesis studies of AHA2 could help to further elucidate the mechanisms involved in the PS mediated stimulation of proton pumping of plant plasma membrane P3 ATPases.

Experimental procedures

Materials. Phospholipids 1-palmitoyl-2-oleoyl-phosphatidylcholine (PC), phosphatidylglycerol (PG), phosphatidylethanolamine (PE), phosphatidylserine (PS), phosphatidic acid (PA), 1,2-dipalmitoyl-*sn*-glycero-3-phosphoethanolamine-N-(7-nitro-2-1,3-benzoxadiazol-4-yl) (N-NBD-PE) were purchased from Avanti Polar Lipids Inc. (Birmingham, AL, USA). N-dodecyl-β-maltoside (DDM) was obtained from Glycon (Luckenwalde, Germany). The ionophores valinomycin and m-chlorophenylhydrazon (CCCP), the pH sensitive dye 9-amino-6-chloro-2-methoxyacridine (ACMA), and all other chemicals and regents were from Sigma-Aldrich (München, Germany), if not stated otherwise. ACMA was dissolved in dimethylsulfoxide; valinomycin in ethanol.

Preparation of Arabidopsis thaliana H$^+$-ATPase Isoform 2. A 73 amino acid C-terminal truncated version of *A. thaliana* H$^+$-ATPase isoform 2 (designated AHA2), containing a hexahistidine (6 × His) and a SNAP® tag at the N-terminal end of the protein, was overexpressed in the *Saccharomyces cerevisiae* strain RS-72 (*MATα, ade1*-100, *his4*-519, *leu2-3*,112) and purified according to previously published protocols (17, 48). All buffers contained 0.2 mM phenylmethylsulfonyl fluoride and 2 µg ml^{-1} pepstatin. The cells were lysed by mixing with glass beads, and the protein was solubilised and purified with DDM at a detergent : protein (w/w) ratio of 1 : 3 using batch-binding to a Ni^{2+}-NTA resin. The purified protein was finally concentrated to 1–10 mg mL^{-1} using centrifugal concentrators with a cut-off at 100 kDa (Vivaspin 100, GE Healthcare), frozen in liquid nitrogen and stored at −80 °C in storage buffer containing 50 mM Mes-KOH (pH 7), 50 mM KCl, 20% (v/v) glycerol, 1 mM EDTA and 1 mM DTT supplemented with 0.04% (w/v) DDM until further use.

Liposome preparation. Liposomes were prepared by re-hydration of a thin lipid film, followed by freeze-thawing and manual extrusion. Briefly, binary lipid mixtures were prepared by mixing appropriate volumes of the lipid stock solutions in chloroform/methanol (2/1, v/v) and trace amounts (0.5 mol%) of fluorescent marker lipid N-NBD-PE in a glass tube. In addition to binary lipid mixtures, a ternary lipid mixture containing 45:45:10 PC:PE:PS was included in the set-up. The solvent was removed using a rotary evaporator (30 min at 200 mbar; 30 min at 100 mbar; 0 mbar for at least 2 h). The lipid film (10 mg) was re-hydrated in 667 µl reconstitution buffer (20 mM MOPS-KOH, pH 7, 50 mM K_2SO_4) by vortexing in the presence of a glass bead (5 mm diameter) for 5 min above phase transition temperature of the lipids (PE 30 °C; for all other room temperature), yielding a final lipid concentration of 15 – 20 mM. The vesicle suspension was further processed by five freeze-thawing cycles (90 s in liquid nitrogen followed by 90 s in a 60°C water bath) and extrusion (21 times) through a stack of polycarbonate membranes (pore size 200 nm) using a mini-extruder (Avanti Polar Lipids). The vesicles made from PC:PE were unstable (lipids felt out of solution after short term storage), possibly because of an increased amount of PE in the membrane and the increased phase transition temperature. Thus, in this case all steps (hydration and extrusion) were performed above 30 °C without storage at 4 °C. Liposome solubilization by octyl glucoside (OG) was monitored by measuring light scattering of the liposome-containing solution at 600 nm using a fluorometer (PTI-Quantamaster 800, Horiba, Benzheim, Germany), thereby determining the 'onset' and 'total' solubilization conditions (49). Detergent was added stepwise (2 µl of 250 mM OG in reconstitution buffer) to the liposome solution and the sample was stirred for 1 min before measuring the scattering. The scattering data as a function of OG concentration was fitted by a Boltzmann equation using a python script to calculate the concentration of OG needed to reach half-way between the saturation and complete solubilization of the vesicles.

$$y = Bottom + \frac{Top - Bottom}{1 + e^{\frac{x - V50}{slope}}}$$

Vesicle reconstitution. To facilitate the insertion of AHA2 into liposomes, preformed liposomes (4 – 5 mM) were solubilized by an amount of OG that was just sufficient to result in a half-maximal scattering change at 600 nm ('Turning Point'). Purified AHA2 (12.5 µg) was added at a protein-to-lipid ratio of 1:60 (w/w). The protein/lipid/detergent mixture was subjected to gel filtration (Sephadex G-50 Fine, 3 ml packed in 2 ml disposable syringes) by centrifugation (180 x g, 8 min). The eluate was incubated for 60 min at room temperature with 50 mg of prewashed SM-2 Bio-Beads (Bio-Rad Laboratories, Hercules, CA, USA) under overhead rotation to ensure detergent removal.

ATP-dependent proton transport assay. H^+ pumping by AHA2 into the vesicles was measured as the initial rate of ACMA fluorescence quenching (50). Proteoliposomes (50 – 200 µM) were added to 987 – 957 µl ACMA buffer (20 mM MOPS-KOH, pH 7.0, 50 mM K_2SO_4, 3 mM ATP, 1 µM ACMA, and 62.5 nM valinomycin). H^+ pumping was initiated by the addition of $MgSO_4$ (3 mM final concentration), and the H^+-gradient dissipated by the addition of 5 µM CCCP. Fluorescence quenching was recorded over a period of 600 s at 480 nm (excitation 412 nm, slit width 2 nm, resolution, 0.1 s) at 23 °C using a PTI-Quantamaster 800. Fluorescence traces were normalized to the intensity measured directly after addition of $MgSO_4$. Recorded traces were analyzed with a customized python script with the slope of a linear curve fitted to the first 50 s after magnesium addition used as a measure for proton pumping activity. Traces, that upon magnesium addition did not show a drop in fluorescence (10% below initial level) were considered inactive and excluded from analysis.

Protein orientation assay. AHA2 orientation in liposomes was determined by site-specific labeling of the SNAP-tag. Proteoliposomes (10 µl, ~ 500 ng AHA2) were incubated for 2 h either sequentially, first with 20 pmol membrane impermeable SNAP dye (10 µM SNAP-Surface® 488, New England BioLabs Inc.) followed by 20 pmol membrane permeable SNAP dye (10 µM SNAP-Cell® 647-SiR, New England BioLabs Inc.) in reconstitution buffer supplemented with 1 mM DTT or with each dye separately. Samples were analyzed by SDS-PAGE using 12% gels and visualized on a ChemiDoc XRS Imaging System (Bio-Rad Laboratories GmbH, München, Germany) using the Image Lab™ software and pre-programmed option for Coomassie stained gels or Alexa488/Alexa647 fluorophores, respectively (51).

Other analytical techniques. Phospholipid phosphorus was assayed after heat destruction in presence of perchloric acid by the method of Bartlett (1959). To check detergent removal and lipid composition, vesicles were analyzed by thin-layer chromatography using chloroform:methanol:ammonium hydroxide (63:35:5, v/v/v). Detergent and lipid standards were chromatographed on the same plate and applied without prior extraction by chloroform/methanol. For visualization, plates were stained with primuline (0.05% in acetone/water, 8/2; v/v) and photographed under long-wave UV light (Biorad ChemiDoc XRS Imaging System).

Data analyses. To analyze the kinetic data, customized algorithms were developted using python version 3.8.8 (52). Data are presented in form of boxplots, with median and 25/75 % quantiles of experiments performed in triplicate, but for statistical analysis the mean ± S.E. One-way analysis of variance was performed using Tukey's honestly significantly differenced (HSD) test employing the python packages scipy.stats (53), statsmodels (54) and bioinfokit (55). The p values <0.05 were interpreted as statistically significant and based on the results

test conditions were grouped, with no statistical significance (ns) within the group, but between groups (ns $p > 0.05$, * $p < 0.05$, ** < 0.01, *** $p < 0.001$).

Molecular dynamics (MD) simulations. For all computational studies the coarse-grain MARTINI 2.2 (56–59) force field was employed. The atomistic structure of AHA2 was retrieved from the protein data bank (PDB) as chain B of entry 5KSD (18), lacking the C-terminal autoregulatory R-domain. The structure was coarse-grained with *martinize 2.6* and an elastic network was applied to stabilize the backbone conformation (60) by connecting backbone beads within a cut-off of 9 Å with harmonic potentials with a force constant of 500 kJ/mol/nm^2. The protein was embedded separately in two lipid bilayers with *insane* (61), containing mixtures of PS:PC (10:90 molar ratio), or PS:PE:PC (10:45:45 molar ratio), respectively. Each bilayer contained 524 lipids in total, distributed symmetrically in both leaflets. All simulations were performed with GROMACS 2020.1 (62–64) at constant temperature (310 K) and pressure (1 bar) using periodic boundary conditions. The two systems were solvated and neutralized with 150 mM NaCl. Each system was energy minimized using steepest-descent and equilibrated with position restraints on all protein beads with a force constant of 1,000 kJ/mol/nm^2. Three 3 µs production runs were started from the equilibrated systems using different random seeds for generating the initial velocities of the particles at 310 K.

The MD parameters used are based on the recommendations of de Jong et al. (65). A leap-frog algorithm was employed for integrating the equations of motion with a time step of 20 fs. Lennard-Jones 6-12 interactions were cut-off after 1.1 nm and shifted to be zero at that interparticle distance. Long-range Coulomb interactions beyond 1.1 nm were treated using a reaction field with the dielectric constant set to infinity. Velocity rescale thermostats with a coupling time constant of 1 ps were applied separately for the protein, the lipid membrane, and the solvent to maintain constant temperature of 310 K. Constant 1 bar pressure was maintained with a Parrinello-Rahman barostat with a coupling constant of 12 ps and compressibility of 0.0003 bar^{-1}, separately for the membrane plane (xy-plane) and its perpendicular axis (z-axis).

MD analyses. Overall translation and rotation of the protein were removed prior to analyses by structural alignment to the starting structure of the simulations. Analyses were conducted for each trajectory separately, and for the concatenated trajectories of the three analogous replicas. Contacts between protein residues and lipid headgroups were analyzed with GROMACS 2020.1 and custom Python scripts. A contact was counted when at least two beads, one from the protein residue and one from a lipid headgroup, were within 0.55 nm from one another and no other lipid was closer to the protein residue. The contacts were normalized by the number of timeframes to obtain the probability of finding a protein-lipid contact at any time. Two-dimensional lipid headgroup densities were computed with the GROMACS tool gmx densmap (grid spacing: 0.02 nm), separately for each leaflet and lipid species. Lastly, three-dimensional lipid densities were computed with MD Analysis (66, 67) considering all PS beads or only PS headgroup beads (grid spacing: 0.1 nm).

Multiple sequence alignment. Protein sequences were downloaded from the UniProt knowledgebase database (access January 2021) and aligned with the tool Clustal Omega (68, 69). Accession numbers are: P20649 and P19456, for the H^+-ATPase isoforms 1 and -2, respectively from *Arabidopsis thaliana*. Q42932, for the H^+-ATPase isoform 2 from *Nicotiana plumbaginifolia*. Q7XPY2, for the H^+-ATPase from *Oryza sativa subsp. Japonica*. P05030, for the H^+-ATPase isoform 1 from *Saccharomyces cerevisiae*. P07038, for the H^+-ATPase from *Neurospora crassa*. P04191, for the SERCA pump from *Oryctolagus cuniculus* and Q4H132, for the Na,K-ATPase from S*qualus acanthias.*

Data availability

All the data are within the article and supporting information. All the data are to be shared upon request.

Supporting information

This article includes supporting information.

Acknowledgements

The authors thank Anne-Mette Bjerg Petersen for excellent technical assistance, Dr. Michael Palmgren for the gifts of yeast plasmids and strain RS-72 and long term support of our research, and Eckhard Hofmann for access to DLS.

Author Contributions

BHJ and TGP conceived the project and supervised the research. LCP conducted all the experiments with assistance of ML and wrote the first version of the manuscript. SH performed MD simulation under supervision of LS and DD. DD performed sequence alignment. All authors performed data analysis, discussed the results and commented on the final manuscript. BHJ, TGP and LS revised the manuscript.

Funding and additional information

This work was funded by grants from the DAAD (57386621) to TGP and the German Research Foundation (SCHA 1574/6-1) to LVS. LCP gratefully acknowledge funding from Studienstiftung des deutschen Volkes.

Conflicts of interest

There are no conflicts to declare. The funders had no role in the design of the study; in the collection, analyses, or interpretation of data; in the writing of the manuscript, or in the decision to publish the results.

References

1. Vinothkumar, K. R., and Henderson, R. (2010) Structures of membrane proteins. *Quart. Rev. Biophys.* **43**, 65–158

2. Gaxiola, R. A., Palmgren, M. G., and Schumacher, K. (2007) Plant proton pumps. *FEBS Letters*. **581**, 2204–2214

3. Kang, J., Park, J., Choi, H., Burla, B., Kretzschmar, T., Lee, Y., and Martinoia, E. (2011) Plant ABC Transporters. *The Arabidopsis Book*. **9**, e0153

4. Axelsen, K. B., and Palmgren, M. G. (1998) Evolution of Substrate Specificities in the P-Type ATPase Superfamily. *J Mol Evol*. **46**, 84–101

5. Axelsen, K. B., and Palmgren, M. G. (2001) Inventory of the Superfamily of P-Type Ion Pumps in Arabidopsis. *Plant Physiology*. **126**, 696–706

6. Palmgren, M. G. (2001) PLANT PLASMA MEMBRANE H^+-ATPases: Powerhouses for Nutrient Uptake. *Annu. Rev. Plant. Physiol. Plant. Mol. Biol.* **52**, 817–845

7. Palmgren, M. G., and Nissen, P. (2011) P-Type ATPases. *Annu. Rev. Biophys.* **40**, 243–266

8. Sondergaard, T. E., Schulz, A., and Palmgren, M. G. (2004) Energization of Transport Processes in Plants. Roles of the Plasma Membrane H^+-ATPase. *Plant Physiology*. **136**, 2475–2482

9. Palmgren, M. G. (1991) Regulation of plant plasma membrane H^+-ATPase activity. *Physiol Plant*. **83**, 314–323

10. Axelsen, K. B., Venema, K., Jahn, T., Baunsgaard, L., and Palmgren, M. G. (1999) Molecular Dissection of the C-Terminal Regulatory Domain of the Plant Plasma Membrane H^+-ATPase AHA2: Mapping of Residues that When Altered Give Rise to an Activated Enzyme. *Biochemistry*. **38**, 7227–7234

11. Wielandt, A. G., Pedersen, J. T., Falhof, J., Kemmer, G. C., Lund, A., Ekberg, K., Fuglsang, A. T., Pomorski, T. G., Buch-Pedersen, M. J., and Palmgren, M. (2015) Specific Activation of the Plant P-type Plasma Membrane H^+-ATPase by Lysophospholipids Depends on the Autoinhibitory N- and C-terminal Domains. *Journal of Biological Chemistry*. **290**, 16281–16291

12. De Michelis, M. I., Papini, R., and Pugliarello, M. C. (1997) Multiple Effects of Lysophosphatidylcholine on the Activity of the Plasma Membrane H^+ -ATPase of Radish Seedlings*. *Botanica Acta*. **110**, 43–48

13. Brauer, D., and Tu, S.-I. (1989) Phospholipid Requirement of the Vanadate-Sensitive ATPase from Maize Roots Evaluated by Two Methods. *Plant Physiol.* **89**, 867–874

14. Serrano, R., Montesinos, C., and Sanchez, J. (1988) Lipid requirements of the plasma membrane ATPases from oat roots and yeast. *Plant Science*. **56**, 117–122

15. Han, X., Yang, Y., Zhao, F., Zhang, T., and Yu, X. (2020) An improved protein lipid overlay assay for studying lipid–protein interactions. *Plant Methods*. **16**, 33

16. Kasamo, K., and Nouchi, I. (1987) The Role of Phospholipids in Plasma Membrane ATPase Activity in *Vigna radiata* L. (Mung Bean) Roots and Hypocotyls. *Plant Physiol.* **83**, 323–328

17. Regenberg, B., Villalba, J. M., Lanfermeijer, F. C., and Palmgren, M. G. (1995) C-terminal deletion analysis of plant plasma membrane H^+-ATPase: yeast as a model system for solute transport across the plant plasma membrane. *Plant Cell*. **7**, 1655–1666

18. Focht, D., Croll, T. I., Pedersen, B. P., and Nissen, P. (2017) Improved Model of Proton Pump Crystal Structure Obtained by Interactive Molecular Dynamics Flexible Fitting Expands the Mechanistic Model for Proton Translocation in P-Type ATPases. *Front. Physiol.* 10.3389/fphys.2017.00202

19. Pedersen, B. P., Buch-Pedersen, M. J., Preben Morth, J., Palmgren, M. G., and Nissen, P. (2007) Crystal structure of the plasma membrane proton pump. *Nature*. **450**, 1111–1114

20. Buch-Pedersen, M. J., Venema, K., Serrano, R., and Palmgren, M. G. (2000) Abolishment of Proton Pumping and Accumulation in the E1P Conformational State of a Plant Plasma Membrane H^+-ATPase by Substitution of a Conserved Aspartyl Residue in Transmembrane Segment 6. *Journal of Biological Chemistry*. **275**, 39167–39173

21. Buch-Pedersen, M. J., and Palmgren, M. G. (2003) Conserved Asp684 in Transmembrane Segment M6 of the Plant Plasma Membrane P-type Proton Pump AHA2 Is a Molecular Determinant of Proton Translocation. *Journal of Biological Chemistry*. **278**, 17845–17851

22. Palmgren, M. G., and Axelsen, K. B. (1998) Evolution of P-type ATPases. *Biochimica et Biophysica Acta (BBA) - Bioenergetics*. **1365**, 37–45

23. Drachmann, N. D., Olesen, C., Møller, J. V., Guo, Z., Nissen, P., and Bublitz, M. (2014) Comparing crystal structures of Ca^{2+}-ATPase in the presence of different lipids. *FEBS J*. **281**, 4249–4262

24. Toyoshima, C., Yonekura, S.-I., Tsueda, J., and Iwasawa, S. (2011) Trinitrophenyl derivatives bind differently from parent adenine nucleotides to Ca^{2+} -ATPase in the absence of Ca^{2+}. *Proc. Natl. Acad. Sci. U.S.A.* **108**, 1833–1838

25. Toyoshima, C., Iwasawa, S., Ogawa, H., Hirata, A., Tsueda, J., and Inesi, G. (2013) Crystal structures of the calcium pump and sarcolipin in the Mg^{2+}-bound E1 state. *Nature*. **495**, 260–264

26. Obara, K., Miyashita, N., Xu, C., Toyoshima, I., Sugita, Y., Inesi, G., and Toyoshima, C. (2005) Structural role of countertransport revealed in Ca^{2+} pump crystal structure in the absence of Ca^{2+}. *Proc. Natl. Acad. Sci. U.S.A.* **102**, 14489–14496

27. Cornelius, F., Habeck, M., Kanai, R., Toyoshima, C., and Karlish, S. J. D. (2015) General and specific lipid–protein interactions in Na,K-ATPase. *Biochimica et Biophysica Acta (BBA) - Biomembranes*. **1848**, 1729–1743

28. Kanai, R., Ogawa, H., Vilsen, B., Cornelius, F., and Toyoshima, C. (2013) Crystal structure of a Na^+-bound Na^+,K^+-ATPase preceding the E1P state. *Nature*. **502**, 201–206

29. Habeck, M., Kapri-Pardes, E., Sharon, M., and Karlish, S. J. D. (2017) Specific phospholipid binding to Na,K-ATPase at two distinct sites. *Proc. Natl. Acad. Sci. U.S.A.* **114**, 2904–2909

30. Athanasopoulos, A., André, B., Sophianopoulou, V., and Gournas, C. (2019) Fungal plasma membrane domains. *FEMS Microbiology Reviews*. **43**, 642–673

31. Addison, R., and Scarborough, G. A. (1981) Solubilization and purification of the Neurospora plasma membrane H^+-ATPase. *Journal of Biological Chemistry*. **256**, 13165–13171

32. Scarborough, G. A. (1977) Properties of the Neurospora crassa plasma membrane ATPase. *Archives of Biochemistry and Biophysics*. **180**, 384–393

33. Hossain, K. R., and Clarke, R. J. (2019) General and specific interactions of the phospholipid bilayer with P-type ATPases. *Biophys Rev*. **11**, 353–364

34. Kasamo, K. (1990) Mechanism for the Activation of Plasma Membrane H^+ -ATPase from Rice (*Oryza sativa* L.) Culture Cells by Molecular Species of a Phospholipid. *Plant Physiol.* **93**, 1049–1052

35. Kasamo, K., and Yamanashi, H. (1991) Functional Reconstitution of Plasma Membrane H^+-ATPase from Mung Bean (Vigna radiata L.) Hypocotyls in Liposomes Prepared with Various Molecular Species of Phospholipids. *Plant and Cell Physiology*. 10.1093/oxfordjournals.pcp.a078200

36. Zhao, P., Zhao, C., Chen, D., Yun, C., Li, H., and Bai, L. (2021) Structure and activation mechanism of the hexameric plasma membrane H^+-ATPase. *Nat Commun*. **12**, 6439

37. Heit, S., Geurts, M. M. G., Murphy, B. J., Corey, R. A., Mills, D. J., Kühlbrandt, W., and Bublitz, M. (2021) Structure of the hexameric fungal plasma membrane proton pump in its autoinhibited state. *Sci. Adv.* **7**, eabj5255

38. Curran, A. C., Hwang, I., Corbin, J., Martinez, S., Rayle, D., Sze, H., and Harper, J. F. (2000) Autoinhibition of a Calmodulin-dependent Calcium Pump Involves a Structure in the Stalk That Connects the Transmembrane Domain to the ATPase Catalytic Domain. *Journal of Biological Chemistry*. **275**, 30301–30308

39. Morsomme, P., Dambly, S., Maudoux, O., and Boutry, M. (1998) Single Point Mutations Distributed in 10 Soluble and Membrane Regions of the Nicotiana plumbaginifolia Plasma Membrane PMA2 H^+-ATPase Activate the Enzyme and Modify the Structure of the C-terminal Region. *Journal of Biological Chemistry*. **273**, 34837–34842

40. Morsomme, P., de Kerchove d'Exaerde, A., De Meester, S., Thinès, D., Goffeau, A., and Boutry, M. (1996) Single point mutations in various domains of a plant plasma membrane H^+-ATPase expressed in Saccharomyces cerevisiae increase H^+-pumping and permit yeast growth at low pH. *The EMBO Journal*. **15**, 5513–5526

41. Merlot, S., Leonhardt, N., Fenzi, F., Valon, C., Costa, M., Piette, L., Vavasseur, A., Genty, B., Boivin, K., Müller, A., Giraudat, J., and Leung, J. (2007) Constitutive activation of a plasma membrane H^+-ATPase prevents abscisic acid-mediated stomatal closure. *EMBO J*. **26**, 3216–3226

42. Kanczewska, J., Marco, S., Vandermeeren, C., Maudoux, O., Rigaud, J.-L., and Boutry, M. (2005) Activation of the plant plasma membrane H^+ -ATPase by phosphorylation and binding of 14-3-3 proteins converts a dimer into a hexamer. *Proc. Natl. Acad. Sci. U.S.A.* **102**, 11675–11680

43. Ekberg, K., Pedersen, B. P., Sørensen, D. M., Nielsen, A. K., Veierskov, B., Nissen, P., Palmgren, M. G., and Buch-Pedersen, M. J. (2010) Structural identification of cation binding pockets in the plasma membrane proton pump. *Proc. Natl. Acad. Sci. U.S.A.* **107**, 21400–21405

44. Rhee, K.-H. (2002) Domain movements of plasma membrane H+-ATPase: 3D structures of two states by electron cryo-microscopy. *The EMBO Journal*. **21**, 3582–3589

45. Ruiz-Granados, Y., De La Cruz-Torres, V., and Sampedro, J. (2019) The Oligomeric State of the Plasma Membrane H^+-ATPase from Kluyveromyces lactis. *Molecules*. **24**, 958

46. Nguyen, T. T., Blackburn, M. R., and Sussman, M. R. (2020) Intermolecular and Intramolecular Interactions of the *Arabidopsis* Plasma Membrane Proton Pump Revealed Using a Mass Spectrometry Cleavable Cross-Linker. *Biochemistry*. **59**, 2210–2225

47. van 't Klooster, J. S., Cheng, T.-Y., Sikkema, H. R., Jeucken, A., Moody, B., and Poolman, B. (2020) Periprotein lipidomes of Saccharomyces cerevisiae provide a flexible environment for conformational changes of membrane proteins. *eLife*. **9**, e57003

48. Cid, A., Perona, R., and Serrano, R. (1987) Replacement of the promoter of the yeast plasma membrane ATPase gene by a galactose-dependent promoter and its physiological consequences. *Curr Genet*. **12**, 105–110

49. Rigaud, J.-L., Pitard, B., and Levy, D. (1995) Reconstitution of membrane proteins into liposomes: application to energy-transducing membrane proteins. *Biochimica et Biophysica Acta (BBA) - Bioenergetics*. **1231**, 223–246

50. Dufour, J. P., Goffeau, A., and Tsong, T. Y. (1982) Active proton uptake in lipid vesicles reconstituted with the purified yeast plasma membrane ATPase. Fluorescence quenching of 9-amino-6-chloro-2-methoxyacridine. *Journal of Biological Chemistry*. **257**, 9365–9371

51. Paweletz, L., Veit, S., and Pomorski, T. (2022) A Fluorescence-based Approach Utilizing Self-labeling Enzyme Tags to Determine Protein Orientation in Large Unilamellar Vesicles. *BIO-PROTOCOL*. 10.21769/BioProtoc.4542

52. Rossum, G. van, and Drake, F. L. (2010) *The Python language reference*, Release 3.0.1 [Repr.], Python documentation manual / Guido van Rossum; Fred L. Drake [ed.], Python Software Foundation, Hampton, NH

53. Virtanen, P., Gommers, R., Oliphant, T. E., Haberland, M., Reddy, T., Cournapeau, D., Burovski, E., Peterson, P., Weckesser, W., Bright, J., van der Walt, S. J., Brett, M., Wilson, J., Millman, K. J., Mayorov, N., Nelson, A. R. J., Jones, E., Kern, R., Larson, E., Carey, C. J., Polat, İ., Feng, Y., Moore, E. W., VanderPlas, J., Laxalde, D., Perktold, J., Cimrman, R., Henriksen, I., Quintero, E. A., Harris, C. R., Archibald, A. M., Ribeiro, A. H., Pedregosa, F., van Mulbregt, P., SciPy 1.0 Contributors, Vijaykumar, A., Bardelli, A. P., Rothberg, A., Hilboll, A., Kloeckner, A., Scopatz, A., Lee, A., Rokem, A., Woods, C. N., Fulton, C., Masson, C., Häggström, C., Fitzgerald, C., Nicholson, D. A., Hagen, D. R., Pasechnik, D. V., Olivetti, E., Martin, E., Wieser, E., Silva, F., Lenders, F., Wilhelm, F., Young, G., Price, G. A., Ingold, G.-L., Allen, G. E., Lee, G. R., Audren, H., Probst, I., Dietrich, J. P., Silterra, J., Webber, J. T., Slavič, J., Nothman, J., Buchner, J., Kulick, J., Schönberger, J. L., de Miranda Cardoso, J. V., Reimer, J., Harrington, J., Rodríguez, J. L. C., Nunez-Iglesias, J., Kuczynski, J., Tritz, K., Thoma, M., Newville, M., Kümmerer, M., Bolingbroke, M., Tartre, M., Pak, M., Smith, N. J., Nowaczyk, N., Shebanov, N., Pavlyk, O., Brodtkorb, P. A., Lee, P., McGibbon, R. T., Feldbauer, R., Lewis, S., Tygier, S., Sievert, S., Vigna, S., Peterson, S., More, S., Pudlik, T., Oshima, T., Pingel, T. J., Robitaille, T. P., Spura, T., Jones, T. R., Cera, T., Leslie, T., Zito, T., Krauss, T., Upadhyay, U., Halchenko, Y. O., and Vázquez-Baeza, Y. (2020) SciPy 1.0: fundamental algorithms for scientific computing in Python. *Nat Methods*. **17**, 261–272

54. Seabold, S., and Perktold, J. (2010) statsmodels: Econometric and statistical modeling with python. *9th Python in Science Conference*

55. Bedre, R. (2020) reneshbedre/bioinfokit: Bioinformatics data analysis and visualization toolkit. 10.5281/ZENODO.3965241

56. de Jong, D. H., Singh, G., Bennett, W. F. D., Arnarez, C., Wassenaar, T. A., Schäfer, L. V., Periole, X., Tieleman, D. P., and Marrink, S. J. (2013) Improved Parameters for the Martini Coarse-Grained Protein Force Field. *J. Chem. Theory Comput.* **9**, 687–697

57. Marrink, S. J., de Vries, A. H., and Mark, A. E. (2004) Coarse Grained Model for Semiquantitative Lipid Simulations. *J. Phys. Chem. B*. **108**, 750–760

58. Marrink, S. J., Risselada, H. J., Yefimov, S., Tieleman, D. P., and de Vries, A. H. (2007) The MARTINI Force Field: Coarse Grained Model for Biomolecular Simulations. *J. Phys. Chem. B*. **111**, 7812–7824

59. Monticelli, L., Kandasamy, S. K., Periole, X., Larson, R. G., Tieleman, D. P., and Marrink, S.-J. (2008) The MARTINI Coarse-Grained Force Field: Extension to Proteins. *J. Chem. Theory Comput.* **4**, 819–834

60. Periole, X., Cavalli, M., Marrink, S.-J., and Ceruso, M. A. (2009) Combining an Elastic Network With a Coarse-Grained Molecular Force Field: Structure, Dynamics, and Intermolecular Recognition. *J. Chem. Theory Comput.* **5**, 2531–2543

61. Wassenaar, T. A., Ingólfsson, H. I., Böckmann, R. A., Tieleman, D. P., and Marrink, S. J. (2015) Computational Lipidomics with *insane* : A Versatile Tool for Generating Custom Membranes for Molecular Simulations. *J. Chem. Theory Comput.* **11**, 2144–2155

62. Pronk, S., Páll, S., Schulz, R., Larsson, P., Bjelkmar, P., Apostolov, R., Shirts, M. R., Smith, J. C., Kasson, P. M., van der Spoel, D., Hess, B., and Lindahl, E. (2013) GROMACS 4.5: a high-throughput and highly parallel open source molecular simulation toolkit. *Bioinformatics*. **29**, 845–854

63. van der Spoel, D., Lindahl, E., Hess, B., Groenhof, G., Mark, A. E., and Berendsen, H. J. C. (2005) GROMACS: Fast, flexible, and free. *J. Comput. Chem.* **26**, 1701–1718

64. Abraham, M. J., Murtola, T., Schulz, R., Páll, S., Smith, J. C., Hess, B., and Lindahl, E. (2015) GROMACS: High performance molecular simulations through multi-level parallelism from laptops to supercomputers. *SoftwareX*. **1–2**, 19–25

65. de Jong, D. H., Baoukina, S., Ingólfsson, H. I., and Marrink, S. J. (2016) Martini straight: Boosting performance using a shorter cutoff and GPUs. *Computer Physics Communications*. **199**, 1–7

66. Gowers, R., Linke, M., Barnoud, J., Reddy, T., Melo, M., Seyler, S., Domański, J., Dotson, D., Buchoux, S., Kenney, I., and Beckstein, O. (2016) MDAnalysis: A Python Package for the Rapid Analysis of Molecular Dynamics Simulations, pp. 98–105, Austin, Texas, 10.25080/Majora-629e541a-00e

67. Michaud-Agrawal, N., Denning, E. J., Woolf, T. B., and Beckstein, O. (2011) MDAnalysis: A toolkit for the analysis of molecular dynamics simulations. *J. Comput. Chem.* **32**, 2319–2327

68. Madeira, F., Park, Y. mi, Lee, J., Buso, N., Gur, T., Madhusoodanan, N., Basutkar, P., Tivey, A. R. N., Potter, S. C., Finn, R. D., and Lopez, R. (2019) The EMBL-EBI search and sequence analysis tools APIs in 2019. *Nucleic Acids Research*. **47**, W636–W641

69. Sievers, F., Wilm, A., Dineen, D., Gibson, T. J., Karplus, K., Li, W., Lopez, R., McWilliam, H., Remmert, M., Söding, J., Thompson, J. D., and Higgins, D. G. (2011) Fast, scalable generation of high-quality protein multiple sequence alignments using Clustal Omega. *Mol Syst Biol*. **7**, 539

70. Pei, J., and Grishin, N. V. (2001) AL2CO: calculation of positional conservation in a protein sequence alignment. *Bioinformatics*. **17**, 700–712

Abbreviations

The abbreviations used are: A-domain, actuator domain; ACMA, 9-amino-6-chloro-2-methoxyacridine; AHA2: *Arabidopsis thaliana* H^+-ATPase isoform 2; CCCP, m-chlorophenylhydrazon; DDM, N-dodecyl-β-maltoside; MD, molecular dynamics; N-NBD-PE, 1,2-dipalmitoyl-*sn*-glycero-3-phosphoethanolamine-N-(7-nitro-2-1,3-benzoxadiazol-4-yl); OG, octyl glucoside; PA, 1-palmitoyl-2-oleoyl-phosphatidic acid; PC, 1-palmitoyl-2-oleoyl-phosphatidylcholine, PE, 1-palmitoyl-2-oleoyl-phosphatidylethanolamine; PG, 1-palmitoyl-2-oleoyl-phosphatidylglycerol; PS, 1-palmitoyl-2-oleoyl-phosphatidylserine; R-domain, autoinhibitory regulatory domain.

Figures and figure legends

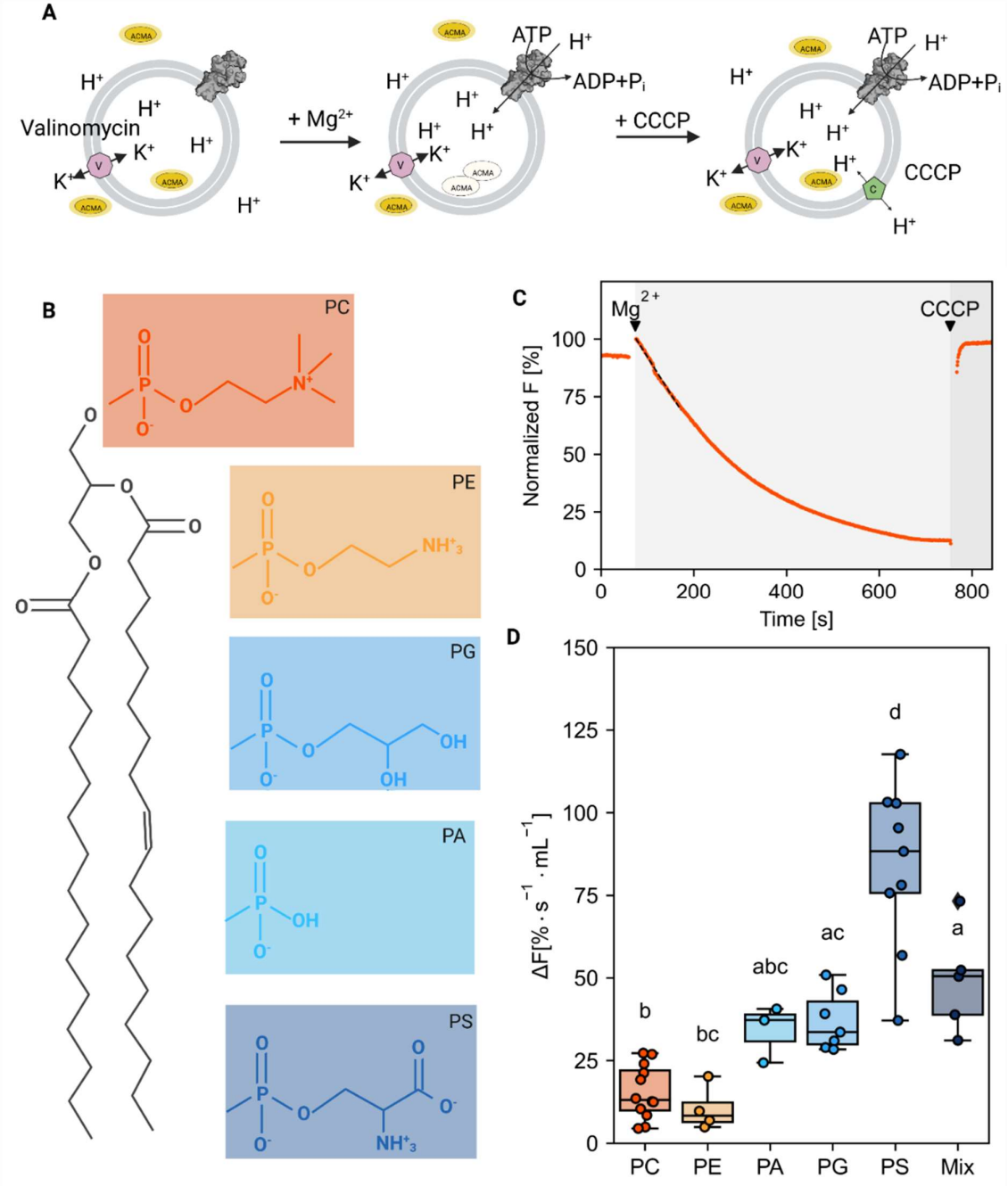

Figure 1. Effect of lipid bilayer composition on AHA2 proton pumping activity. (A) Illustration of the proton pumping assay on proteoliposomes with reconstituted AHA2. The accumulation of protons inside the vesicles was determined by measuring the fluorescence quenching of ACMA as a fluorescent ΔpH probe. Reactions were started by the addition of Mg^{2+} to ATP-containing buffer. After reaching saturation conditions, the H^+ gradient was disrupted by the addition of the protonophore CCCP. Valinomycin was always present to mediate K^+ exchange and prevent the build-up of a transmembrane electrical potential. (B) Lewis structures of the lipids used. (C) Representative ACMA fluorescence trace on proteoliposomes with reconstituted H^+-ATPase. The initial slope (dashed line) was taken as a measure for the proton pumping rate. (D) Dot plot showing the initial rates of proton pumping of AHA2

reconstituted in liposomes composed of pure PC and PC in mixture with the indicated phospholipids (30 mol%); the mix contained PC:PE:PS (45:45:10). Letters above box plots indicate significant differences determined by Tukey's HSD test ($P<0.05$). Box plot center lines show the medians. Box limits indicate the 25th and 75th percentiles. Whiskers are extended to the highest and the lowest values. Data are based on at least three independent reconstitutions measured three times (see number of reconstitutions in Suppl. Tab.1).

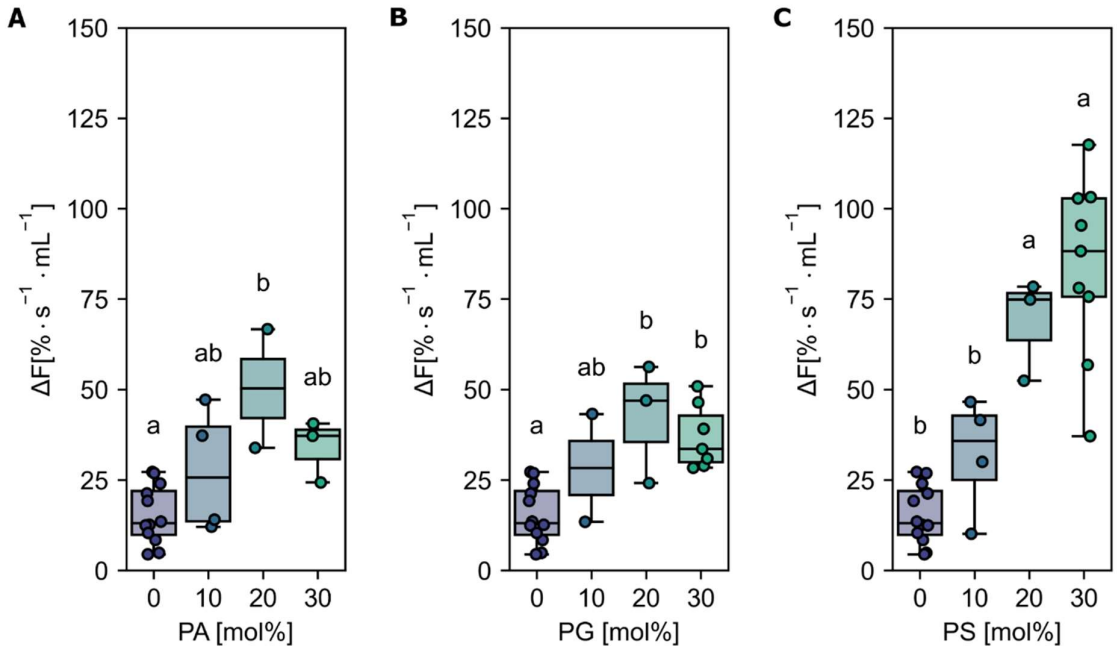

Figure 2. Effect of anionic lipids on AHA2 activity in proteoliposomes. AHA2 was reconstituted into liposomes composed of PC in mixture with the indicated amounts of anionic lipids, namely PA (A), PG (B) and PS (C). Dot plots show the initial rates of proton pumping. 0 and 30 mol% are listed for comparison and are the same data sets as in Figure 1. Letters above box plots indicate significant differences determined by Tukey's HSD test ($P<0.05$). Box plot center lines show the medians. Box limits indicate the 25th and 75th percentiles. Whiskers are extended to the highest and the lowest values. Data are based on at least two independent reconstitutions measured two to four times (see number of reconstitutions in Suppl. Tab.2 - 4).

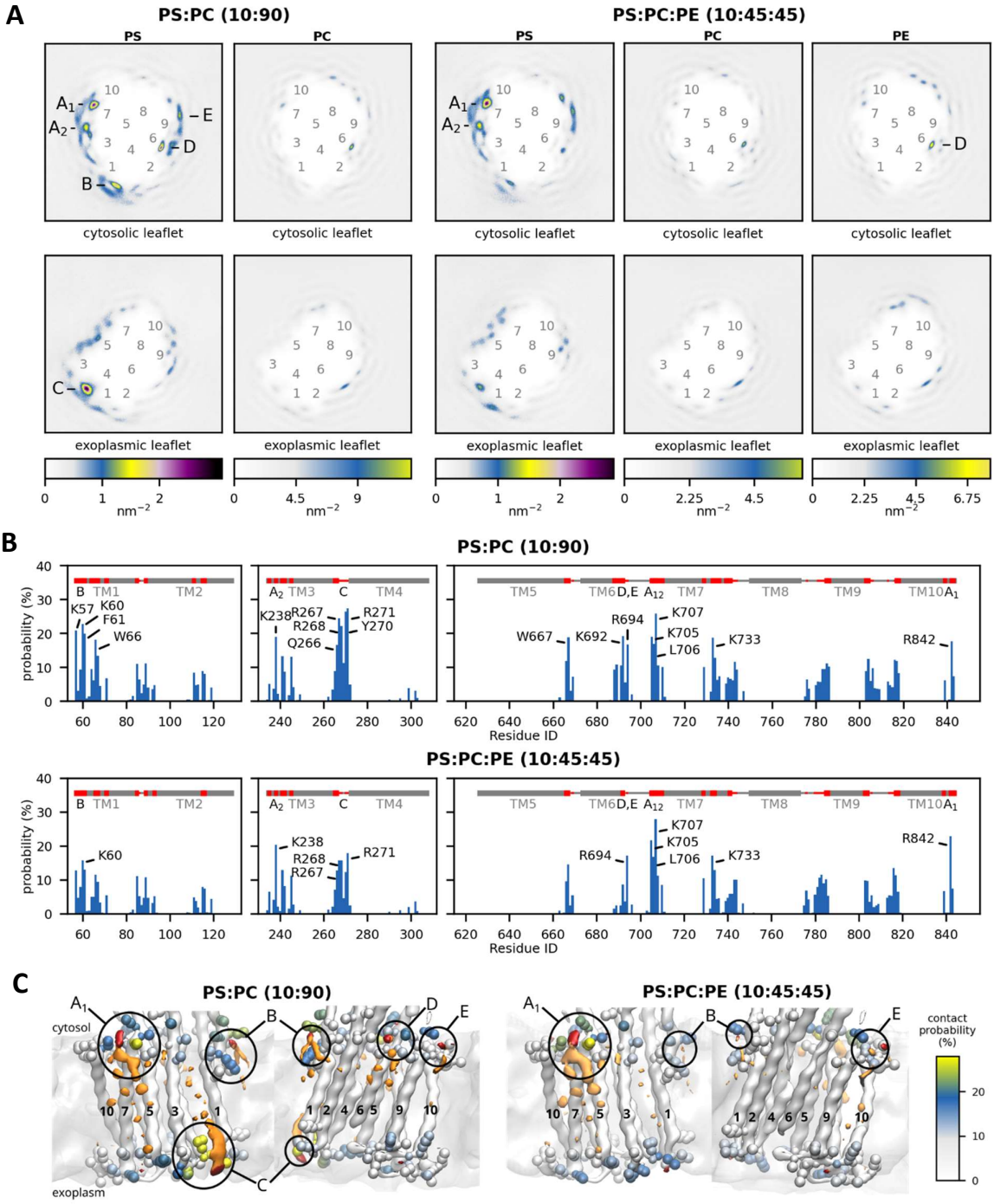

Figure 3. Phospholipid-AHA2 interactions from MD simulations. **(A)** Two-dimensional density of lipid headgroups, plotted separately for each leaflet. The color scales (bottom) are adjusted such that they reflect the molar ratio of the different lipid species in the bilayer. Labels 1-10 mark the approximate locations of the transmembrane helices; labels A-E mark local density maxima. **(B)** Contact probabilities of individual AHA2 residues with PS headgroups. Residues with contact probabilities above 15% are labeled. The secondary structure of AHA2 is depicted in grey at the top, with residues with ≥5% contact probability colored red and corresponding density maxima labeled A-E. **(C)** Protein-lipid interaction sites are shown from two perspectives, with isosurfaces of the three-dimensional density of PS headgroup beads shown in red (isovalue 3 nm^{-3}) and the rest of PS in orange (isovalue 4 nm^{-3}). AHA2 residues with ≥5% lipid contacts are shown as beads, colored by contact probability (color bar at the right). The density maxima A-E are labeled.

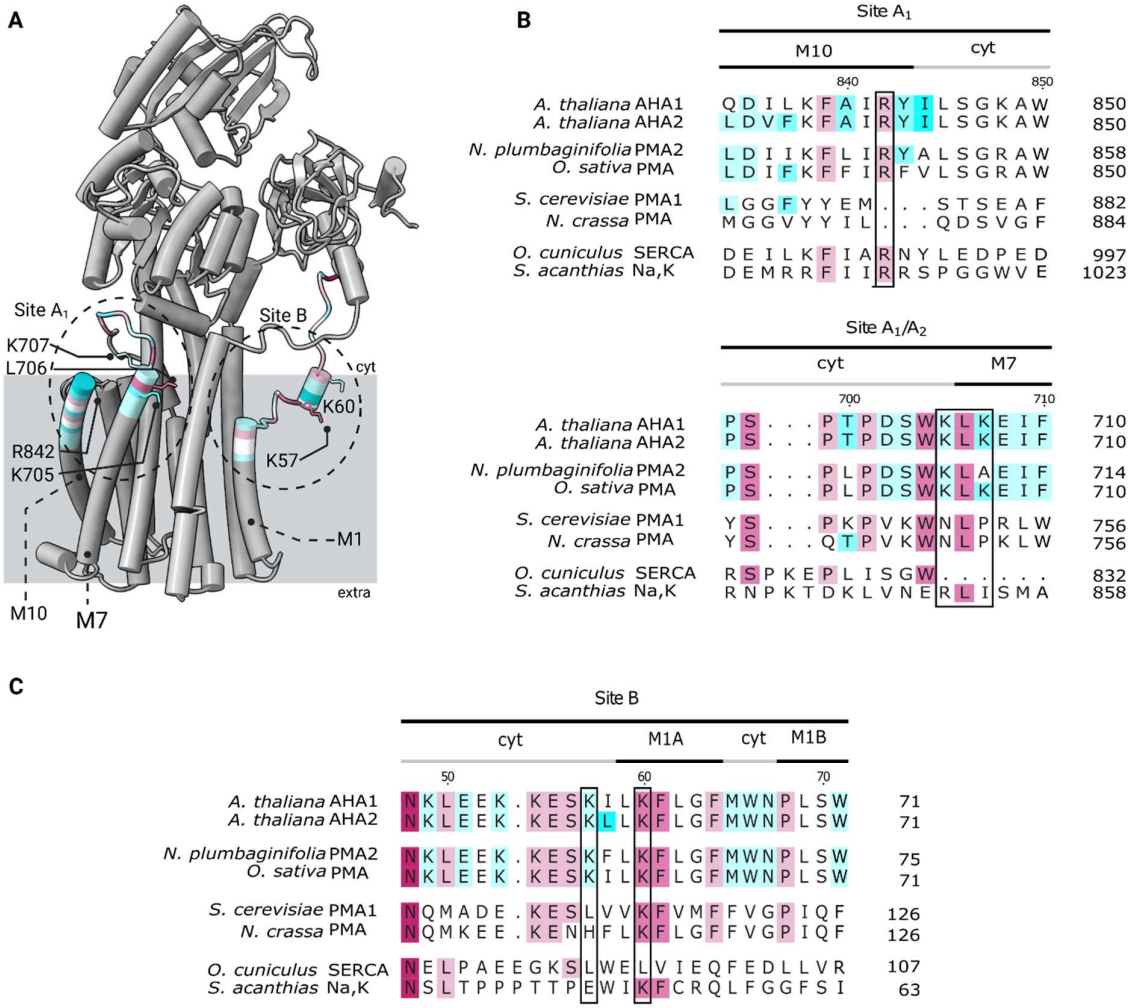

Figure 4. Location of predicted anionic phospholipid contact sites A_1 and B in AHA2 and their sequence alignment in related P-type ATPases. (A) Cartoon representation of the AHA2. Patches of apprx. 15 residues around the assigned contact residues are colored according to their sequence conservation based on AL2CO algorithm implemented into ChimeraX (70). Preferentially interacting residues identified in the lipid-protein contact analysis are shown in atom representation. The approximate regions of the anionic lipid contacts sites, as identified in the lipid density maps, are marked with black, dashed circles. (B, C) Sequence alignment showing the conservation of residues based on AL2CO algorithm in selected P-type ATPase proton pumps from plants and yeasts as well as SERCA and Na,K-ATPase at the regions of the two selected anionic lipid contact sites identified in AHA2 (sites A1 and B). The sequences were obtained from the Uniprot database: *Arabidopsis thaliana* H^+-ATPase isoform 1-2 (P20649 and P1945), shown in the first block, followed by the plant proton pumps *Nicotiana plumbaginifolia* H^+-ATPase isoform 2 *(Q42932), Oryza sativa subsp. Japonica* H^+-ATPase *(Q7XPY2),* and the two fungal transporters (*Saccharomyces cerevisiae* H^+-ATPase isoform 1 (P05030), *Neurospora crassa* H^+-ATPase (P07038). Lastly, they are compared to the SERCA pump from rabbit Oryctolagus cuniculus (P04191) and the Na,K-ATPase from shark Squalus acanthias (Q4H132). Residues in black boxes are found to have enriched lipid contacts in the MD simulations.